Plasma pressure in Mercury's equatorial magnetosphere derived from MESSENGER Magnetometer observations

Haje Korth,[1] Brian J. Anderson,[1] Jim M. Raines,[2] James A. Slavin,[2] Thomas H. Zurbuchen,[2] Catherine L. Johnson,[3,4] Michael E. Purucker,[5] Reka M. Winslow,[3] Sean C. Solomon,[6] and Ralph L. McNutt Jr.[1]

Received 29 August 2011; revised 11 October 2011; accepted 17 October 2011; published 17 November 2011.

[1] Since insertion of the MErcury Surface, Space ENvironment, GEochemistry, and Ranging (MESSENGER) spacecraft into orbit around Mercury on 18 March 2011, the probe's Magnetometer has routinely observed localized reductions of the magnetic field magnitude below the level predicted by a planetary dipole model corrected for magnetospheric magnetic fields. These magnetic depressions are observed on almost every orbit, and the latitude at which they are observed is local-time dependent. The depression signatures are indicators of the presence of enhanced plasma pressures, which inflate the magnetic field locally to maintain pressure balance, thus lowering the magnetic flux density. Mapping the magnetic depressions in local time and latitude provides insight into the plasma distribution near the planet, which complements that provided by MESSENGER's Fast Imaging Plasma Spectrometer. The spatial distribution shows that magnetic depressions are concentrated in two distinct regions, one near the equator on the nightside and another at high latitudes principally on the dayside. Here we focus on the nightside, equatorial pressure signatures, which we attribute to the magnetotail plasma sheet. The plasma-sheet pressures extend from dusk to dawn and are offset northward from the planetary geographic equator by about 10° in latitude, commensurate with the offset of the planetary dipole. The pressures associated with the plasma-sheet depressions range from 0.1 to 3 nPa and are systematically higher at dawn than at dusk. Proton gradient-curvature and convection drift in Mercury's dipole magnetic field with a dawn-to-dusk electric field result in low drift velocities near dawn, leading to systematically higher densities and pressures at dawn than at dusk, consistent with the observations. **Citation:** Korth, H., B. J. Anderson, J. M. Raines, J. A. Slavin, T. H. Zurbuchen, C. L. Johnson, M. E. Purucker, R. M. Winslow, S. C. Solomon, and R. L. McNutt Jr. (2011), Plasma pressure in Mercury's equatorial magnetosphere derived from MESSENGER Magnetometer observations, *Geophys. Res. Lett.*, *38*, L22201, doi:10.1029/2011GL049451.

[1]The Johns Hopkins University Applied Physics Laboratory, Laurel, Maryland, USA.
[2]Department of Atmospheric, Oceanic and Space Sciences, University of Michigan, Ann Arbor, Michigan, USA.
[3]Department of Earth and Ocean Sciences, University of British Columbia, Vancouver, British Columbia, Canada.
[4]Planetary Science Institute, Tucson, Arizona, USA.
[5]Solar System Exploration Division, NASA Goddard Space Flight Center, Greenbelt, Maryland, USA.
[6]Department of Terrestrial Magnetism, Carnegie Institution of Washington, Washington, DC, USA.

0094-8276/11/2011GL049451

1. Introduction

[2] In a planetary magnetosphere, the circulation of magnetic flux and plasma from the sub-solar reconnection site into the nightside magnetotail and back to the dayside is a fundamental process termed the Dungey cycle [*Dungey*, 1961]. Under an adiabatic approximation, the drift velocity, $\boldsymbol{v}_{\mathbf{D}}$, of a charged particle is governed by the electric, $\boldsymbol{E}$, and magnetic, $\boldsymbol{B}$, fields:

$$\boldsymbol{v}_{\mathbf{D}} = \frac{\boldsymbol{E}\times\boldsymbol{B}}{B_2} + \frac{m\,v_{\perp}^2}{2\,q\,B^2}(\boldsymbol{B}\times\nabla B) + \frac{m\,v_{\parallel}^2}{q}\frac{\boldsymbol{R}_c\times\boldsymbol{B}}{R_c^2 B^2}, \qquad (1)$$

where m and q are the mass and charge of the particle, $v_{\perp}$ and $v_{\parallel}$ are the components of the particle velocity perpendicular and parallel to $\boldsymbol{B}$, and $\boldsymbol{R}_c$ is the local radius of curvature of the magnetic field lines [e.g., *Baumjohann and Treumann*, 1997]. The drift terms in equation (1) are termed the $\boldsymbol{E}\times\boldsymbol{B}$, gradient, and curvature drifts, respectively. In magnetospheres with a southward-directed planetary dipole moment, such as those of Earth and Mercury, electrons (positive ions) drift eastward (westward) around the planet. For electrons and positive ions, the electric and magnetic drift terms are oppositely directed at dusk and dawn, respectively. The relative importance of the electric and magnetic drifts depends on the particle energy, so that the direction of motion is eastward for lower-energy ions, whereas higher-energy ions drift westward around the planet. The statistical distribution of plasma in the terrestrial magnetosphere is well documented and is consistent with the drift paradigm [*Wing and Newell*, 1998; *Korth et al.*, 1999; *Friedel et al.*, 2001; *Wang et al.*, 2006].

[3] With the insertion of the MErcury Surface, Space ENvironment, GEochemistry, and Ranging (MESSENGER) spacecraft into orbit about Mercury on 18 March 2011, our understanding of magnetospheric dynamics can be tested under conditions not found at Earth. The higher reconnection efficiency and smaller magnetotail diameter of Mercury's magnetosphere result in stronger cross-tail electric fields [*Slavin et al.*, 2009], whereas electric fields associated with co-rotation of plasma near the planet's surface are negligible because of Mercury's long, 59 day, rotation period. In addition, the surface equatorial magnetic field at Mercury is more than two orders of magnitude weaker than that of Earth [*Ness et al.*, 1975; *Alexeev et al.*, 2010; *Anderson et al.*, 2011]. Consequently, the relative magnitudes of electric and magnetic drifts for Earth and Mercury differ, and this difference should be reflected in the distribution of magnetospheric plasmas.

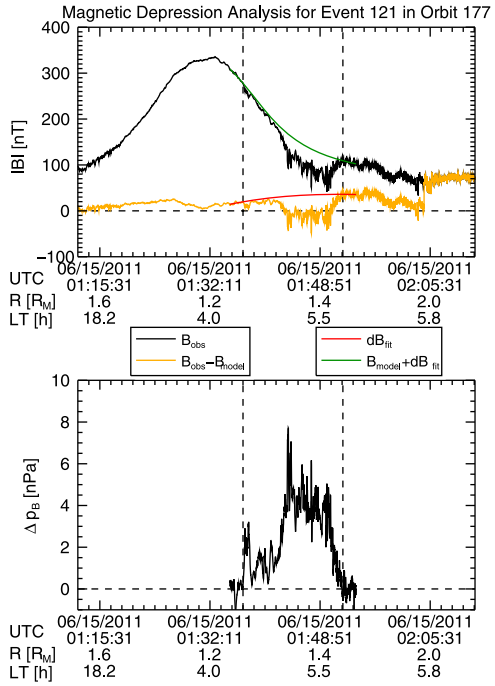

Figure 1. Magnetic depression event observed on 15 June 2011. (top) Time series of the magnitudes of the observed magnetic field (black), model residual magnetic field (orange), baseline magnetic field fit (red), and model magnetic field corrected with the baseline fit (green). (bottom) Time series of the magnetic pressure deficit. In both panels, the interval boundaries of the depression events are marked by vertical dashed lines. R is the radial distance from the planet center, and LT denotes local time.

[4] Our present understanding of the plasma distribution in Mercury's magnetosphere is based to a large extent on results from magnetohydrodynamic [*Kabin et al.*, 2000; *Benna et al.*, 2010], kinetic hybrid [*Kallio and Janhunen*, 2003; *Trávníček et al.*, 2007, 2009, 2010], and large-scale kinetic simulations [*Delcourt et al.*, 2003; *Mura et al.*, 2005]. With the advent of MESSENGER orbital operations, it is now possible to characterize the plasma structure of the magnetosphere observationally. To facilitate investigation of magnetospheric plasmas, MESSENGER is equipped with a Magnetometer (MAG) [*Anderson et al.*, 2007] and the Fast Imaging Plasma Spectrometer (FIPS), one of two sensors on the Energetic Particle and Plasma Spectrometer (EPPS) [*Andrews et al.*, 2007]. Here we use MAG data to locate plasma populations through the characteristic magnetic signatures produced by their thermal pressure. We present the first statistical picture of the equatorial plasma distribution in Mercury's magnetosphere derived from MAG orbital observations and demonstrate good qualitative correspondence with FIPS proton data. The findings are interpreted in terms of particle drifts, i.e., in the adiabatic limit.

2. Observations and Analysis

[5] MESSENGER's near-polar orbit has a periapsis altitude of 200 km, an inclination of 82.5°, an apoapsis altitude of 15,300 km, and a nominal orbit period of 12 hours. MAG observations have been acquired near continuously since 23 March 2011, and complete coverage in magnetic local time has since been achieved, with some local times having been sampled more than once. The vector magnetic field is obtained by MAG at rates of 20 or 2 samples per second dependent on location along the orbit and available data downlink rates. In this study we use 1-s averages of these data. As an example, observations of the magnetic field magnitude for a 1-h interval near the periapsis transit during orbit 177 with the descending node at local dawn are shown in Figure 1 (top). The planet's intrinsic magnetic field, given by a spin-axis-aligned, southward-directed dipole of moment 195 nT R_M^3, where R_M = 2440 km is Mercury's radius, and a 484-km northward offset along the spin axis [*Anderson et al.*, 2011], is clearly evident in Figure 1. Superposed on the dipole magnetic field are localized reductions of the magnetic field magnitude, B, which are observed both on the ascending and the descending nodes of the orbit. MESSENGER has encountered such magnetic depressions on almost every orbit, although the latitude at which they are observed is local-time dependent.

[6] The magnetic depression signatures are attributed to neither the planetary dipole nor the large-scale magnetospheric current systems, but are instead indicators of the presence of enhanced plasma pressures. The total pressure is given by the sum of magnetic and kinetic pressures, so that an increase in one of these contributions must be balanced by a decrease in the other to maintain constant total pressure. Because the magnetic pressure is proportional to B^2, the pressure associated with the plasma population can be determined by the deficit in the magnetic field magnitude with respect to the undisturbed baseline. To evaluate the reduction in magnetic pressure, we first subtracted the model magnetic field of *Alexeev et al.* [2008, 2010], consisting of the internal dipole field determined by *Anderson et al.* [2011] and an external magnetic field due to magnetospheric current systems. For the magnetospheric magnetic fields, a best-

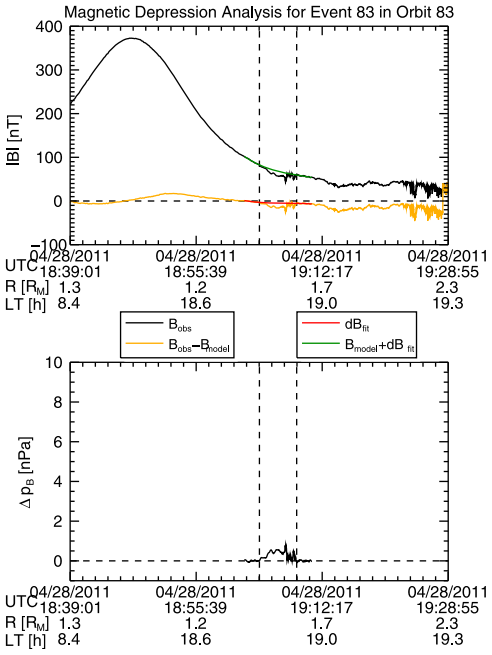

Figure 2. Magnetic depression event observed on 28 April 2011 shown in the same format as in Figure 1.

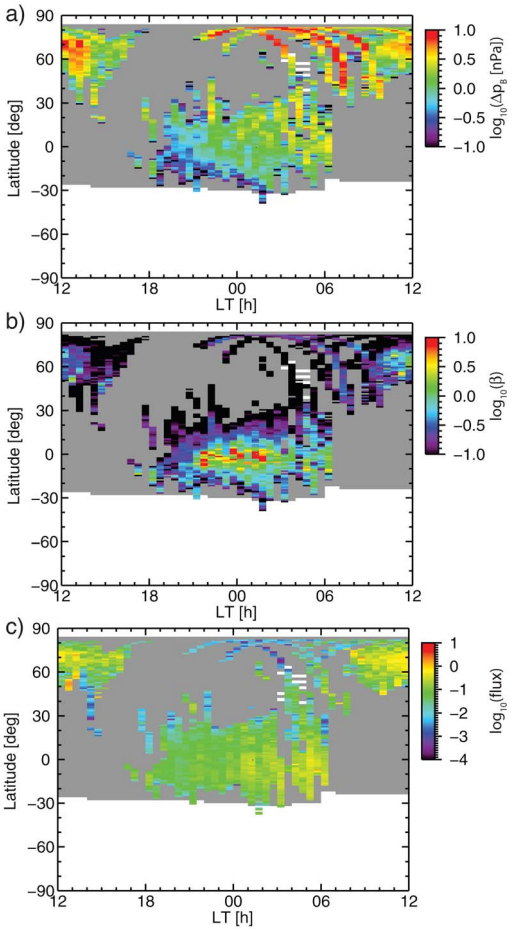

Figure 3. Distribution of the logarithm to base 10 of (a) the magnetic pressure deficit magnitude, (b) the plasma β as function of magnetic local time and latitude, and (c) the normalized proton flux as measured by FIPS, as functions of magnetic local time and latitude.

estimate parameterization from orbital and flyby magnetic field observations was applied. We used a subsolar magnetopause stand-off distance of 1.4 R_M, a magnetopause flaring factor of 1, a tail current sheet having a thickness of 0.5 R_M and an inner edge located at 1.32 R_M radial distance from the planet center, and a lobe magnetic field of 100 nT. The beginning and end of each depression interval are easily identified in the residual magnetic field (Figure 1, top) as negative perturbations from the baseline often accompanied by strong fluctuations. We then fit the magnetic field baseline using up to 2 min of data on either side of the magnetic field depression interval with a third-order polynomial and corrected the model magnetic field with the fit result. Finally, the magnetic pressure deficit, Δp_B, was computed from

$$\Delta p_B = \left[(B_m + \Delta B_m)^2 - B^2\right]/(2\mu_0), \qquad (2)$$

where B_m is the model magnetic field, ΔB_m is the fitted model residual, and μ_0 is the magnetic permeability of free space. The magnitude of Δp_B for the observations in Figure 1 (top), shown in Figure 1 (bottom), exhibits reductions in magnetic pressure by up to 8 nPa. In contrast, Figure 2 shows a similar analysis for orbit 83, for which the descending node of the orbit is at dusk. The magnetic depression and corresponding pressure deficit (<1 nPa) are substantially smaller than observed for the dawn-side event. The prevalence of strong magnetic depressions at dawn and comparatively weak depressions at dusk is a consistent feature of the orbital data.

[7] To quantify the distribution of enhanced plasma pressures, we mapped and averaged the computed Δp_B magnitudes for events observed through 25 July 2011, a total of 284 events, in magnetic local time and latitude in 0.5-h and 1°-wide bins, respectively, to yield a comprehensive picture of the plasma pressure distribution near the planet. The resulting map, shown in Figure 3a, shows that magnetic depressions are concentrated in two distinct regions. The first, of primary interest here, is approximately centered about the magnetic equator on the nightside, generally restricted to magnetic local times between 1800 and 0600 hours, and typically not observed on the dayside. The spatial extent of this population is indicative of the plasma sheet in the equatorial magnetotail. The second region of magnetic depression signatures is at high latitudes, predominantly on the dayside, and may be associated with the northern magnetospheric cusp. The bin averages of the pressure deficit magnitude range between 0.1 and 3 nPa in the equatorial region and reach up to 10 nPa at high latitudes. The high-latitude events are not treated further in this study.

[8] In the terrestrial magnetosphere, plasma pressures of similar magnitudes are observed in the magnetotail plasma sheet and in the inner equatorial region, where their gradients give rise to diamagnetic currents, $J = (\boldsymbol{B} \times \nabla p)/B^2$. To evaluate the relative importance of such currents to the dynamics of Mercury's magnetosphere, we compute the plasma β, i.e., the ratio of the thermal pressure, p_{th}, to the magnetic pressure: $\beta = 2\mu_0 p_{th}/B^2$. In doing so we assume that the thermal pressure equals the magnetic pressure deficit computed above: $p_{th} = \Delta p_B$. Figure 3b shows β as function of magnetic local time and latitude. The plasma population near the nightside equatorial plane corresponds to β from unity up to 10, consistent with values for the terrestrial nightside plasma sheet [*Borovsky et al.*, 1997].

[9] The MAG observations of magnetic field depressions attributed to plasma pressures are complementary to the observation of ions by FIPS. The FIPS field of view spans a solid angle of ~1.4π sr, so that one cannot ensure that the measured portion of the ion distributions are always sufficient to derive the distribution moments reliably. Nonetheless, the MAG-derived pressure distribution should be correlated with the FIPS ion fluxes. The FIPS proton fluxes acquired during the magnetic depression events and normalized with respect to accumulation time and geometric factor are shown as functions of magnetic local time and latitude in Figure 3c. Comparison shows that both the FIPS proton fluxes and pressure depressions exhibit enhancements at dayside high-latitudes and near the magnetic equator on the nightside.

3. Discussion and Conclusions

[10] A prominent feature in the pressure and flux distributions associated with the plasma sheet is a gradient directed from dusk to dawn demonstrating that both pressure and proton fluxes in the nightside equatorial plane are higher at dawn than at dusk at the altitudes sampled by

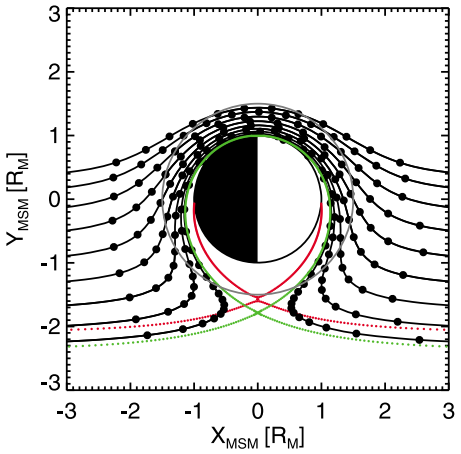

Figure 4. Drift trajectories of equatorially mirroring protons having energies of 5 keV at a radial distance of 1.5 R_M (grey circle) in the magnetic equatorial plane. The separatrices between open and closed drift paths, i.e., the Alfvén layers, for 3- and 5-keV protons are shown as red and green lines, respectively. The time ticks along the trajectories are spaced at 10 s intervals.

MESSENGER. For similar temperatures across the magnetic tail, this result also implies that the proton density is higher at dawn than at dusk. In Earth's magnetosphere, where the dipole field has the same orientation as at Mercury, positive ions are observed to drift duskward [*Korth et al.*, 1999], so that one would expect higher ion fluxes in the dusk-side magnetosphere, whereas at Mercury we observe the opposite. To explain the reason for this difference, we consider a simple Hamiltonian energy-conservation approach [*Whipple*, 1978; *Korth et al.*, 1999] to model the drifts of protons in a dipolar magnetic field and the electric field imposed on the magnetosphere by the solar wind and the co-rotation of plasma near the planetary surface (negligible for Mercury) [*Volland*, 1973; *Stern*, 1975; *Volland*, 1975, 1978]. This approach is applicable to particles that conserve the first two adiabatic invariants associated with gyro and bounce motion of the particle around and along a magnetic field line, respectively. To test the validity of the approach, we computed the adiabaticity parameter $\kappa = \sqrt{R_{min}/\rho_{max}}$, where R_{min} is the minimum curvature radius of the magnetic field line and ρ_{max} is the maximum proton Larmor radius [*Büchner and Zelenyi*, 1989]. The regime of adiabatic transport is given by $\kappa > 3$ [*Delcourt and Martin*, 1994]. Computation of κ in the nightside equatorial region sampled by MESSENGER with the magnetospheric magnetic field model described above yields $2 < \kappa < 4$ (see auxiliary material), which is near the limit of validity for the guiding-center-drift assumption but should allow a first investigation of the MESSENGER observations.[1] Furthermore, typical plasma sheet energies observed by FIPS at Mercury are about 5 keV [*Zurbuchen et al.*, 2011], for which the gyro-radius of a proton at the magnetic equator, where the magnetic field magnitude at an altitude of ~1000 km is ~100 nT [*Anderson et al.*, 2011], is ~100 km. These protons can thus gyrate about magnetic field lines without colliding with the planet's surface. The bounce period for a near-equatorial-mirroring 5-keV proton is about 20 s [*Schulz and Lanzerotti*, 1974], which is somewhat long compared with the Dungey-cycle period of ~2 min [*Slavin et al.*, 2010], so our calculations are for equatorially mirroring protons. For the particle simulation, the magnetic field is parameterized as noted above. The cross-polar electric potential drop was estimated from Mercury flyby observations to be 30 kV, which yields a mean dawn-to-dusk electric field of ~2 mV/m [*Slavin et al.*, 2009] and which is four orders of magnitude larger than the corotation potential (2×10^{-3} kV).

[11] Drift trajectories of equatorially mirroring protons with an energy of 5 keV at a radial distance of 1.5 R_M in the magnetic equatorial plane are shown in Figure 4 in Mercury solar magnetic (MSM) coordinates, where $+X$ is sunward, $+Y$ is duskward, and $+Z$ is northward. The grey circle shows the approximate location of MESSENGER intersections with the magnetic equator. Consistent with the electric field, protons drift from the nightside magnetotail to the dayside magnetopause in 1–2 min. On the dawn side, protons drift closer to the stagnation point, where electric and magnetic drifts are of equal magnitude but oppositely directed, leading to higher densities than at dusk. We suggest that the longer dwell time enhances the proton density near dawn, thus explaining the dusk-to-dawn gradient observed in the distributions of both the differential magnetic pressure and the proton flux. Furthermore, since the displacement in the Y direction tailward of the observing locations is similar for all drift trajectories, the energy gains in convection across the tail are comparable for all drift paths crossing the MESSENGER orbit intersection with the magnetic equator, so that the pressure variations should be predominantly due to density differences. The behavior of particle drifts inward of where MESSENGER transits the equator is considered further below. Similar density enhancements have been observed in Earth's magnetosphere by *Korth et al.* [1999] at geosynchronous orbit and *Wing and Newell* [1998]. The latter authors observed dawn-side enhancements in the proton densities primarily during active conditions, when the eastward electric drift is enhanced relative to the westward-directed magnetic drifts. As a result, more protons are delivered to the dawn region, where they slow near the stagnation point, thus increasing the density. At Mercury, because of the strong cross-tail electric field, the electric drift velocity dominates at all times, so that the phenomenon is persistent at Mercury. It is conceivable that the dawn-side plasma enhancement is not restricted to protons but also applies to heavy-ion species. Such a feature has been predicted to exist from Na^+ transport simulations in Mercury's magnetosphere [*Yagi et al.*, 2010] and has been observed in the terrestrial magnetosphere for O^+ by *Ohtani et al.* [2011].

[12] Although the drift calculations indicate that Mercury's weak magnetic field and strong convection may account for the observations, more detailed modeling and simulations to test this hypothesis should address a number of other considerations. The actual magnetic field at Mercury is markedly modified from that of a dipole, even close to the planet, by the magnetopause and cross-tail current systems, so a more rigorous calculation should include more complete models for the total magnetic field. At Earth, the Alfvén layers are associated with electric-field shielding of the inner magnetosphere from the dawn-to-dusk electric field. Whether this

[1] Auxiliary materials are available in the HTML. doi:10.1029/2011GL049451.

shielding occurs at Mercury is not known. Nor do we fully understand the appropriate electromagnetic boundary condition to apply at the planetary surface, an issue that would need to be resolved before undertaking more sophisticated drift calculations. Finally, the northward displacement of Mercury's dipole from the geographic equator implies that the precipitation loss cones at equatorial altitudes sampled by MESSENGER will be large, because particles with pitch angles smaller than 30° to 45° will encounter the planetary surface in the southern hemisphere. As a result, plasma-sheet distribution functions are likely to exhibit large temperature anisotropies, which in turn will drive wave-particle instabilities that promote pitch-angle scattering. This scattering will result in greater precipitation loss, which will deplete the plasma as ions drift duskward across the tail close to the planet [*Delcourt et al.*, 2003]. Additional losses are anticipated for lower-energy ions in the dawn-side magnetosphere, because those ions cannot be diverted around the planet to the dayside. The geometry of the Alfvén layer of 3-keV protons intercepting the planet surface near the noon–midnight meridian (Figure 4) suggests that a substantial fraction of protons entering on the dawn side will drift into the planetary surface even without pitch angle scattering by waves. The precipitation and drift losses may also contribute to the dawnward-directed pressure gradient [*Delcourt et al.*, 2003; *Yagi et al.*, 2010]. Detailed analyses of actual proton distribution functions and observed pitch-angle distributions together with more complete models and simulations will be required to identify the relative importance of these additional factors governing plasma dynamics at Mercury. Such analyses must also be extended to the dominant heavy-ion species for which the above loss mechanisms have been demonstrated through single-particle simulations [*Delcourt et al.*, 2003; *Yagi et al.*, 2010]. Nonetheless, it seems clear that the combination of a relatively weak magnetic field and strong convection yields a plasma sheet that is qualitatively different from that at Earth.

[13] **Acknowledgments.** The MESSENGER project is supported by the NASA Discovery Program under contracts NAS5-97271 to the Johns Hopkins University Applied Physics Laboratory and NASW-00002 to the Carnegie Institution of Washington. CLJ and RW acknowledge support from NSERC.

[14] The Editor thanks Anna Milillo and an anonymous reviewer for their assistance in evaluating this paper.

References

Alexeev, I. I., E. S. Belenkaya, S. Y. Bobrovnikov, J. A. Slavin, and M. Sarantos (2008), Paraboloid model of Mercury's magnetosphere, *J. Geophys. Res.*, *113*, A12210, doi:10.1029/2008JA013368.

Alexeev, I. I., et al. (2010), Mercury's magnetospheric magnetic field after the first two MESSENGER flybys, *Icarus*, *209*, 23–39, doi:10.1016/j.icarus.2010.01.024.

Anderson, B. J., M. H. Acuña, D. A. Lohr, J. Scheifele, A. Raval, H. Korth, and J. A. Slavin (2007), The Magnetometer instrument on MESSENGER, *Space Sci. Rev.*, *131*, 417–450, doi:10.1007/s11214-007-9246-7.

Anderson, B. J., C. L. Johnson, H. Korth, M. E. Purucker, R. M. Winslow, J. A. Slavin, S. C. Solomon, R. L. McNutt, Jr., J. M. Raines, and T. H. Zurbuchen (2011), The global magnetic field of Mercury from MESSENGER orbital observations, *Science*, *333*, 1859–1862, doi:10.1126/science.1211001.

Andrews, G. B., et al. (2007), The Energetic Particle and Plasma Spectrometer instrument on the MESSENGER spacecraft, *Space Sci. Rev.*, *131*, 523–556, doi:10.1007/s11214-007-9272-5.

Baumjohann, W., and R. A. Treumann (1997), *Basic Space Plasma Physics*, 329 pp., Imp. Coll. Press, London.

Benna, M., et al. (2010), Modeling of the magnetosphere of Mercury at the time of the first MESSENGER flyby, *Icarus*, *209*, 3–10, doi:10.1016/j.icarus.2009.11.036.

Borovsky, J. E., R. C. Elphic, H. O. Funsten, and M. F. Thomsen (1997), The Earth's plasma sheet as a laboratory for flow turbulence in high-beta MHD, *J. Plasma Phys.*, *57*, 1–34, doi:10.1017/S0022377896005259.

Büchner, J., and L. M. Zelenyi (1989), Regular and chaotic charged-particle motion in magnetotail-like field reversals: 1. Basic theory of trapped motion, *J. Geophys. Res.*, *94*, 11,821–11,842, doi:10.1029/JA094iA09p11821.

Delcourt, D. C., and R. F. Martin (1994), Application of the centrifugal impulse model to particle motion in the near-Earth magnetotail, *J. Geophys. Res.*, *99*, 23,583–23,590, doi:10.1029/94JA01845.

Delcourt, D. C., S. Grimald, F. Leblanc, J. J. Berthelier, A. Millilo, A. Mura, S. Orsini, and T. E. Moore (2003), A quantitative model of the planetary Na^+ contribution to Mercury's magnetosphere, *Ann. Geophys.*, *21*, 1723–1736, doi:10.5194/angeo-21-1723-2003.

Dungey, J. W. (1961), Interplanetary magnetic field and auroral zones, *Phys. Rev. Lett.*, *6*, 47–48, doi:10.1103/PhysRevLett.6.47.

Friedel, R. H. W., H. Korth, M. G. Henderson, M. F. Thomsen, and J. D. Scudder (2001), Plasma sheet access to the inner magnetosphere, *J. Geophys. Res.*, *106*, 5845–5858, doi:10.1029/2000JA003011.

Kabin, K., T. I. Gombosi, D. L. DeZeeuw, and K. G. Powell (2000), Interaction of Mercury with the solar wind, *Icarus*, *143*, 397–406, doi:10.1006/icar.1999.6252.

Kallio, E., and P. Janhunen (2003), Modelling the solar wind interaction with Mercury by a quasi-neutral hybrid model, *Ann. Geophys.*, *21*, 2133–2145, doi:10.5194/angeo-21-2133-2003.

Korth, H., M. F. Thomsen, J. E. Borovsky, and D. J. McComas (1999), Plasma sheet access to geosynchronous orbit, *J. Geophys. Res.*, *104*, 25,047–25,061, doi:10.1029/1999JA900292.

Mura, A., S. Orsini, A. Milillo, D. Delcourt, S. Massetti, and E. De Angelis (2005), Dayside H^+ circulation at Mercury and neutral particle emission, *Icarus*, *175*, 305–319, doi:10.1016/j.icarus.2004.12.010.

Ness, N. F., K. W. Behannon, R. P. Lepping, and Y. C. Whang (1975), Magnetic field of Mercury, 1, *J. Geophys. Res.*, *80*, 2708–2716, doi:10.1029/JA080i019p02708.

Ohtani, S., M. Nose, S. P. Christon, and A. T. Y. Lui (2011), Energetic O^+ and H^+ ions in the plasma sheet: Implications for the transport of ionospheric ions, *J. Geophys. Res.*, *116*, A10211, doi:10.1029/2011JA016532.

Schulz, M., and L. J. Lanzerotti (1974), *Particle Diffusion in the Radiation Belts*, *Phys. Chem. Space*, vol. 7, 215 pp., Springer, New York.

Slavin, J. A., et al. (2009), MESSENGER observations of magnetic reconnection in Mercury's magnetosphere, *Science*, *324*, 606–610, doi:10.1126/science.1172011.

Slavin, J. A., et al. (2010), MESSENGER observations of extreme loading and unloading of Mercury's magnetic tail, *Science*, *329*, 665–668, doi:10.1126/science.1188067.

Stern, D. P. (1975), The motion of a proton in the equatorial magnetosphere, *J. Geophys. Res.*, *80*, 595–599, doi:10.1029/JA080i004p00595.

Trávníček, P. M., P. Hellinger, and D. Schriver (2007), Structure of Mercury's magnetosphere for different pressure of the solar wind: Three-dimensional hybrid simulations, *Geophys. Res. Lett.*, *34*, L05104, doi:10.1029/2006GL028518.

Trávníček, P. M., P. Hellinger, D. Schriver, D. Herčík, J. A. Slavin, and B. J. Anderson (2009), Kinetic instabilities in Mercury's magnetosphere: Three-dimensional simulation results, *Geophys. Res. Lett.*, *36*, L07104, doi:10.1029/2008GL036630.

Trávníček, P. M., D. Schriver, P. Hellinger, D. Herčík, B. J. Anderson, M. Sarantos, and J. A. Slavin (2010), Mercury's magnetosphere-solar wind interaction for northward and southward interplanetary magnetic field: Hybrid simulation results, *Icarus*, *209*, 11–22, doi:10.1016/j.icarus.2010.01.008.

Volland, H. (1973), Semiempirical model of large-scale magnetospheric electric fields, *J. Geophys. Res.*, *78*, 171–180, doi:10.1029/JA078i001p00171.

Volland, H. (1975), Models of global electric fields within the magnetosphere, *Ann. Geophys.*, *31*, 159–173.

Volland, H. (1978), Model of magnetospheric electric convection field, *J. Geophys. Res.*, *83*, 2695–2699, doi:10.1029/JA083iA06p02695.

Wang, C. P., L. R. Lyons, J. M. Weygand, T. Nagai, and R. W. McEntire (2006), Equatorial distributions of the plasma sheet ions, their electric and magnetic drifts, and magnetic fields under different interplanetary magnetic field B_z conditions, *J. Geophys. Res.*, *111*, A04215, doi:10.1029/2005JA011545.

Whipple, E. C. (1978), (*U*, *B*, *K*) coordinates: A natural system for studying magnetospheric convection, *J. Geophys. Res.*, *83*, 4318–4326, doi:10.1029/JA083iA09p04318.

Wing, S., and P. T. Newell (1998), Central plasma sheet ion properties as inferred from ionospheric observations, *J. Geophys. Res.*, *103*, 6785–6800, doi:10.1029/97JA02994.

Yagi, M., K. Seki, Y. Matsumoto, D. C. Delcourt, and F. Leblanc (2010), Formation of a sodium ring in Mercury's magnetosphere, *J. Geophys. Res.*, *115*, A10253, doi:10.1029/2009JA015226.

Zurbuchen, T. H., et al. (2011), MESSENGER observations of the spatial distribution of planetary ions near Mercury, *Science*, *333*, 1862–1865, doi:10.1126/science.1211302.

B. J. Anderson, H. Korth, and R. L. McNutt, Jr., The Johns Hopkins University Applied Physics Laboratory, Laurel, MD 20723, USA. (haje.korth@jhuapl.edu)

C. L. Johnson and R. M. Winslow, Department of Earth and Ocean Sciences, University of British Columbia, 6339 Stores Rd., Vancouver, BC V6T 1Z4, Canada.

M. E. Purucker, Solar System Exploration Division, NASA Goddard Space Flight Center, Greenbelt, MD 20771, USA.

J. M. Raines, J. A. Slavin, and T. H. Zurbuchen, Department of Atmospheric, Oceanic and Space Sciences, University of Michigan, Ann Arbor, MI 48109, USA.

S. C. Solomon, Department of Terrestrial Magnetism, Carnegie Institution of Washington, Washington, DC 20015, USA.